Available online at www.sciencedirect.com

SciVerse ScienceDirect

Ceramics International 38 (2012) 3039–3046

CERAMICS INTERNATIONAL

www.elsevier.com/locate/ceramint

Evaluation of $(Ba_{0.5}Sr_{0.5})_{0.85}Gd_{0.15}Co_{0.8}Fe_{0.2}O_{3-\delta}$ cathode for intermediate temperature solid oxide fuel cell

Zhongqiu Li [a,b,*], Bo Wei [a], Zhe Lü [a], Yaohui Zhang [a], Kongfa Chen [c], Jipeng Miao [a], Wenhui Su [a,d]

[a] Center for the Condensed-Matter Science and Technology, Department of Physics, Harbin Institute of Technology, Harbin 150001, PR China
[b] Heilongjiang Key Laboratory for Low Dimensional System Mesoscopic Physic, School of Physics and Electronic Engineering, Harbin Normal University, Harbin 150025, PR China
[c] Fuels and Energy Technology Institute, Department of Chemical Engineering, Curtin University, Perth, WA 6102, Australia
[d] International Center for Material Physics, Chinese Academy of Sciences, Shenyang 110015, PR China

Received 17 October 2011; received in revised form 1 December 2011; accepted 1 December 2011
Available online 8 December 2011

Abstract

A perovskite-type $(Ba_{0.5}Sr_{0.5})_{0.85}Gd_{0.15}Co_{0.8}Fe_{0.2}O_{3-\delta}$ (BSGCF) oxide has been investigated as the cathode of intermediate temperature solid oxide fuel cells (IT-SOFCs). Coulometric titration, thermogravimetry analysis, thermal expansion and four-probe DC resistance measurements indicate that the introduction of Gd^{3+} ions into the A-site of $Ba_{0.5}Sr_{0.5}Co_{0.8}Fe_{0.2}O_{3-\delta}$ (BSCF) leads to the increase in both oxygen nonstoichiometry at room temperature and electrical conductivity. For example, the conductivity of BSGCF is 148 S cm^{-1} at 507 °C, over 4 times as large as that of BSCF. Furthermore, the electrochemical activity toward the oxygen reduction reaction is also enhanced by the Gd doping. Impedance spectra conducted on symmetrical half cells show that the interfacial polarization resistance of the BSGCF cathode is 0.171 Ω cm^2 at 600 °C, smaller than 0.297 Ω cm^2 of the BSCF cathode. A Ni/$Sm_{0.2}Ce_{0.8}O_{1.9}$ anode-supported single cell based on the BSGCF cathode exhibits a peak power density of 551 mW cm^{-2} at 600 °C.

Keywords: Solid oxide fuel cells (SOFCs); BSGCF; Thermogravimetric analysis; Thermal expansion; Electrical conductivity

1. Introduction

Solid oxide fuel cells (SOFCs) have attracted considerable attention due to its high energy conversion efficiency and low pollution. From the viewpoint of practical application, the traditional high temperature SOFCs operating at 800–1000 °C confront many challenges such as high costs, materials incompatibility and long term stability [1,2]. Significant efforts have been made to develop intermediate temperature SOFC (500–800 °C) [3]. On the other hand, reducing the operating temperature slows down the electrode kinetics process inevitably and results in large interfacial polarization resistances [4]. Therefore, it is essential to develop alternative cathode materials with high electrochemical activity at intermediate temperature to enhance the cell performance. $La_{1-x}Sr_xCoO_{3-\delta}$ has been studied as the candidate materials for IT-SOFCs, as it exhibits excellent mixed electronic/ionic conductivity over a wide temperature range [5–8]. However, it is chemically and thermally incompatible with YSZ and these problems restrict its application in IT-SOFCs [9].

In recent years, $Ba_{0.5}Sr_{0.5}Co_{0.8}Fe_{0.2}O_{3-\delta}$ (BSCF) with high catalytic activity and good oxygen permeability at reduced temperatures has been intensively investigated [10–13]. However, the electrical conductivity of BSCF at 550 °C is only 32 S cm^{-1} [14,15], an order of magnitude lower than 350 S cm^{-1} of $La_{0.6}Sr_{0.4}Co_{0.2}Fe_{0.8}O_3$ (LSCF) [16]. A high electrical conductivity for a cathode facilitates fast electron transfer and thereby improves electrochemical activity for oxygen reduction reaction on the cathode. Researchers have made efforts to enhance the electrical conductivity of BSCF by addition of components with a higher conductivity, such as Ag network within the electrode [17,18] and combining BSCF with other cathode materials that have a higher conductivity such as (La,Sr)MnO_3 and (Sm,Sr)CoO_3 [19,20]. Li et al. [21–23] reported that the

* Corresponding author at: Center for the Condensed-Matter Science and Technology, Department of Physics, Harbin Institute of Technology, Harbin, 150001, PR China. Tel.: +86 461 86418420; fax: +86 461 86418420.
E-mail address: lvzhe@hit.edu.cn (Z. Li).

0272-8842/$36.00
doi:10.1016/j.ceramint.2011.12.001

introduction of rare earths (La, Sm, and Nd) in the A-site of BSCF resulted in both enhanced electrical conductivity and electrochemical behavior toward oxygen reduction reaction.

In the present study, Gd was introduced to the A-site of BSCF to form a new $(Ba_{0.5}Sr_{0.5})_{0.85}Gd_{0.15}Co_{0.8}Fe_{0.2}O_{3-\delta}$ (BSGCF) oxide via a modified sol–gel method. A comparative study between the BSGCF and BSCF is carried out by investigating the phase structure, oxygen nonstoichiometry δ, thermogravimetry (TG) and electrical conductivity. The electrochemical impedance spectra were investigated on symmetrical half cells. The feasibility of the BSGCF cathode was demonstrated on an anode supported single cell.

2. Experimental

2.1. Synthesis of oxide powders

A modified sol–gel method was used to synthesize the $(Ba_{0.5}Sr_{0.5})_{0.85}Gd_{0.15}Co_{0.8}Fe_{0.2}O_{3-\delta}$ (BSGCF) and $Ba_{0.5}Sr_{0.5}Co_{0.8}Fe_{0.2}O_{3-\delta}$ (BSCF) [24]. BSGCF was made from $Ba(NO_3)_2$, $Sr(NO_3)_2$, $Co(NO_3)_2{\cdot}6H_2O$, $Fe(NO_3)_3{\cdot}9H_2O$ and Gd_2O_3 that was dissolved by diluted nitric acid. The nitrates were dissolved in de-ionized water, followed by stirring and heating. EDTA and citric acid were added to the solution and the molar ratio of metal ions: EDTA: citric acid was adjusted to 1:1:1.5. $NH_3{\cdot}H_2O$ was then applied to adjust the pH value of the solution to around 6 to prevent precipitation. After being heat-treated at 180 °C overnight in an oven, the primary composite oxides were calcined at 1000 °C in air for 5 h.

$Sm_{0.2}Ce_{0.8}O_{1.9}$ (SDC) electrolyte powder was made from cerium nitrate, samarium oxide and citric acid by the sol–gel method. The ratio of metal ions: citric acid was 1:1.5. The resulting gel was held at 180 °C for several hours to form dry gel. After calcination at 850 °C for 2 h, the oxide powders were characterized by X-ray diffraction.

2.2. Materials characterization

X-ray diffraction (XRD, Rigaku *D*/max rB PC2550, Japan) patterns of the powder samples were carried out using Cu Kα radiation ($\lambda = 0.15418$ nm), and the diffraction angle is from 10° to 90° with a step of 0.02°. The room temperature oxygen contents $(3-\delta)$ of the BSGCF and BSCF were determined using a coulometric titration technique [25].

The oxygen loss as a function of temperature was measured by the thermogravimetry (TG) using a TA SDT2960 thermal analysis system. The powder samples were heated from 50 to 900 °C at a ramping rate of 10 °C min^{-1} with an air flow rate of 100 ml min^{-1}. Combined with titration results, the nonstoichiometry at high temperature can be obtained. Dense samples were prepared by uniaxially pressing and sintering. The densities of the samples were tested by the Archimedes method. Only the samples with relative density of over 90% were selected for the thermal expansion and electrical conductivity measurements. Thermal expansion coefficients (TECs) of the sintered samples were measured by a Netzsch DIL402C/3/G dilatometer during steady heating (5 °C min^{-1}) from room temperature to 900 °C with air as purge gas (flow rate: 50 ml min^{-1}). Rectangular samples (9 mm × 4 mm × 1 mm) were prepared for electrical conductivities measurement. The test was carried out by the standard four-probe method in air using a Keithley 2400 digital sourcemeter. The testing temperature was ranged from 50 °C to 800 °C with heating and cooling rates of 8 °C min^{-1}.

2.3. Symmetrical cell performance

Symmetrical half-cell configuration was used for the cathode electrochemical performance evaluation. The SDC powder was compacted followed by sintering at 1400 °C for 4 h to obtain dense pellets of 12 mm in diameter and 0.55 mm in thickness. The cathode slurry was prepared by mixing BSGCF or BSCF with an organic vehicle (ethyl cellulose and terpineol). The slurry was coated symmetrically on both sides of the SDC pellets, followed by calcining at 1000 °C for 4 h in air. The effective area of the cathodes was ~0.28 cm^2 and the cathode had a thickness of ~10 μm. Silver paste (DAD-87, Shanghai Research Institute of Synthetic Resin) was painted on the electrodes as current collector. The electrochemical measurements were performed from 500 to 650 °C using an electrochemical system including an electrochemical interface (Solartron SI 1287) and an Impedance/Gain-phase Analyzer (Solartron SI 1260). The impedance spectra were tested in the frequency range from 0.1 Hz to 91 kHz with a signal amplitude of 10 mV under open-circuit conditions. The impedance spectra were fitted using ZView 2.3f software. The microstructures of the (BSCF or BSGCF)/SDC half-cell were studied by SEM.

2.4. Anode-supported single cell evaluation

NiO, SDC and wheat starch were mixed at a weight ratio of 65:35:20 as anode powders. The mixture was pestled in a mortar for 2 h and then pressed into pellets of 13 mm in diameter at a uniaxial pressure of 200 MPa, followed by calcining at 1000 °C for 2 h. Anode functional layers (AFL) which consisted of NiO and SDC at a weight ratio of 6:4 and SDC films were consecutively deposited on the anode substrates by slurry spin coating [26,27], followed by sintering at 1400 °C for 4 h. Finally, BSGCF slurry was printed onto the SDC films and sintered at 1000 °C for 2 h.

Fuel cells were tested with a four-probe method. The cell was sealed onto one end of an alumina tube. The cell was heated in a furnace gradually to 600 °C and the NiO in the anode was reduced to Ni in situ by hydrogen. The anode was fed with 50 ml min^{-1} dry hydrogen and the cathode was exposed to the ambient air. *I–V* curves and AC impedance spectra of the fuel cell were measured using an electrochemical interface Solartron SI 1287 and an impedance analyzer SI 1260.

3. Results and discussion

3.1. Crystal structure

XRD patterns of the BSCF and BSGCF are shown in Fig. 1. Both the powders exhibit a cubic perovskite structure with a

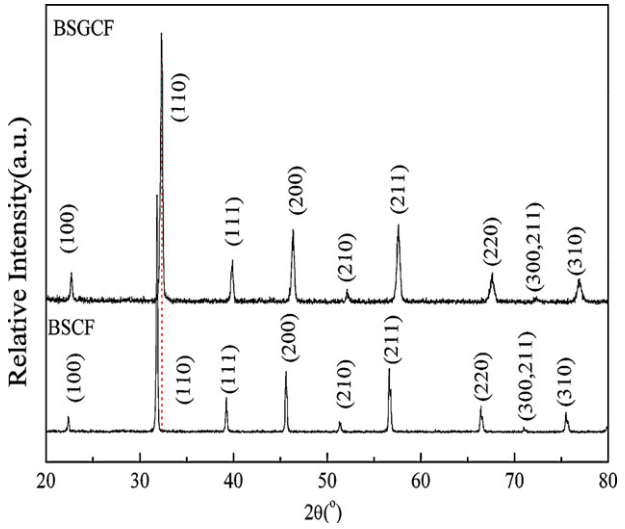

Fig. 1. Powder X-ray diffraction patterns of BSCF and BSGCF oxides.

space group of *Pm3m* [28]. After the introduction of Gd, the main peak (1 1 0) shifts from 31.84° for BSCF to 32.32° for BSGCF. The shifting indicates that the Gd-doping causes the lattice shrinkage of BSCF. This is understandable because the ion radius of Gd^{3+} (0.1277 nm) is smaller than both of those of Ba^{2+} (0.175 nm) and Sr^{2+} (0.158 nm). Moreover, as both Ba and Sr in the A-site are bivalent, the introduction of the Gd^{3+} could reduce the valence states of Co and Fe in the B-site. The reduction of the valence state in the B-site and the concomitant generation of oxygen vacancies affect the lattice (see below).

3.2. Oxygen nonstoichiometry analysis

Table 1 shows the oxygen nonstoichiometries of the BSCF and BSGCF oxides tested at room temperature. A larger oxygen nonstoichiometry δ for BSGCF is observed due to the existence of Gd^{3+} in the A-site. Partial substitution of Ba^{2+} and Sr^{2+} by Gd^{3+} results in the reduction of the valence state in the B-site to maintain the electrical neutrality. The quantity of Co^{4+} and Fe^{4+} in BSGCF is therefore smaller than that of BSCF.

Thermogravimetric (TG) analysis of BSCF and BSGCF compositions are performed in air at elevated temperatures. Fig. 2a shows the weight loss during heating. Fig. 2b shows the oxygen nonstoichiometries $(3-\delta)$ of BSCF and BSGCF oxides. The room temperature values were determined by the coulometric titration and the higher-temperature values were obtained from the TG results. As shown in Fig. 2a, the weight of both the samples starts to decrease at ~350 °C and continuously decreases up to 900 °C, accompanied by the loss of oxygen and the reduction of Co^{4+} and Fe^{4+}. The weight loss of BSGCF at 900 °C is ~1.1%, smaller than ~1.5% of BSCF. This is consistent with the result of coulometric titration, which demonstrates that the quantity of Co^{4+} and Fe^{4+} in BSGCF is smaller than that of BSCF. Chen et al. [29] also observed that the weight loss was about 1.5% at 900 °C in the $Ba_{0.5}Sr_{0.5}Co_{1-y}Fe_yO_{3-\delta}$ compounds with $y = 0.2$. The decrease in the weight loss indicates that the Gd-doping in the A-site slightly affects the valence states of Co and Fe in the B-site. This reasoning is supported by the fact that there is only slight difference between the oxygen nonstoichiometry δ values at high temperature for BSCF and BSGCF oxides (Fig. 2b). The oxygen stoichiometry $(3-\delta)$ of BSCF in this study is 2.896, higher than 2.674 and 2.55 of BSCF with the same composition reported by Chen et al. [29] and by Jung et al. [30], respectively. The synthesis method, calcination temperature and test

Table 1
The room temperature oxygen nonstoichiometries $(3-\delta)$ for BSCF and BSGCF.

Samples	Oxygen content (3-δ)	Average valence of B-site	The ratio of B^{3+}/B^{4+}
BSCF	2.896	3.792	0.263:1
BSGCF	2.875	3.6	0.667:1

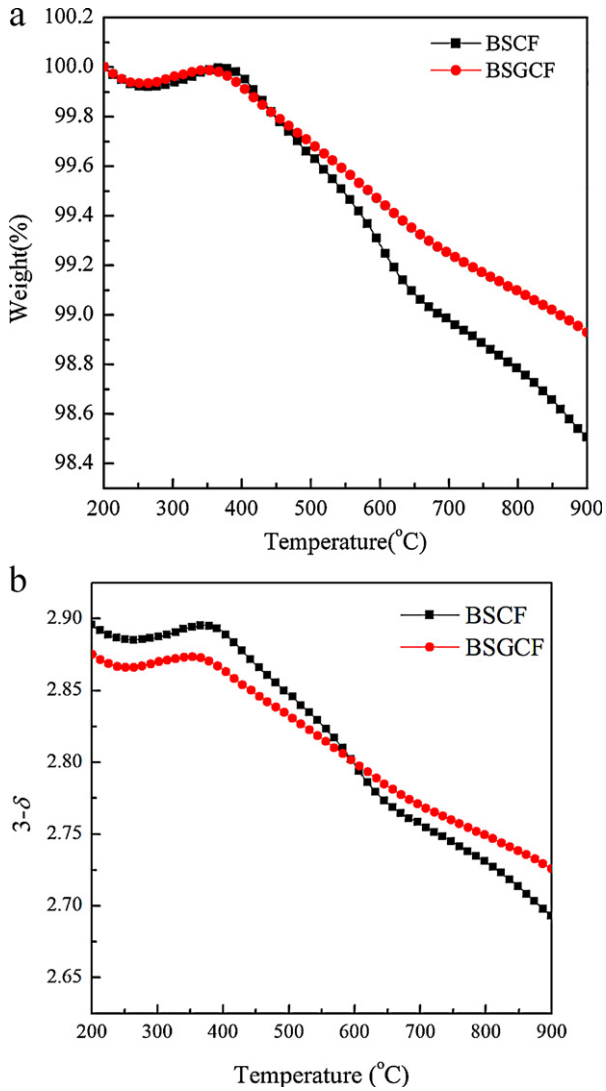

Fig. 2. Temperature dependence of weight loss (a) and the oxygen content (b), for BSCF and BSGCF oxides.

conditions are most likely responsible for the observed discrepancy.

3.3. Thermal expansion

The thermal expansion measurements for BSCF and BSGCF were carried out in the temperature range of 50–900 °C in air. Fig. 3 shows the thermal expansion behaviors and the corresponding technical thermal expansion coefficient. They show linear dependences with temperature in the range of 50–400 °C and 500–900 °C, respectively. A nonlinear thermal expansion occurs from 400 to 500 °C. The chemical expansion observed at high temperature in the cubic materials is a result of reduction of Co/Fe(IV) to the larger Co/Fe (III) ion, increasing the oxygen nonstoichiometry and thus lowering the strength of the chemical bonds in the material [31]. Combined with prior results as shown in Table 1, the oxygen nonstoichiometry $(3-\delta)$ of BSGCF is smaller than of BSCF. So less Co/Fe (IV) was reduced into Co/Fe (III) with increasing temperature in BSGCF sample, which is the prime cause of smaller TEC for BSGCF. The average TECs in whole temperature range are $20.7 \times 10^{-6}\ K^{-1}$ for BSCF and $19.8 \times 10^{-6}\ K^{-1}$ for BSGCF, respectively.

3.4. Electrical conductivity

The electrical conductivities and the Arrhenius curves of the cathodes are plotted in Figs. 4 and 5, respectively. The conductivities of both the samples increase firstly, reach a maximum, and then decrease with increasing temperature. The maximum electrical conductivity appears at a higher temperature for BSGCF as compared to that of BSCF. The maximum conductivity of BSGCF is 148 S cm^{-1} at 507 °C, over 4 times as large as that of BSCF at 450 °C.

The observed increase of the electrical conductivity of BSCF with Gd doping is attributed to two reasons. The conductivity in BSGCF can be ascribed to the hopping of *p*-type small polarons, as proved by thermoelectric method [14,32]. The introduction of Gd^{3+} in A-site induces the reduction of Fe^{4+} and Co^{4+} in the B-site. Thus the ratio of B^{3+}/B^{4+} in BSGCF increases as a result of the charge compensation and it results in increase of the number of current carrier. This reason is supported by the results of room-temperature oxygen non-stoichiometry. The doping of Gd^{3+} in BSCF has a positive effect on the electrical conductivity. Fig. 5 shows the Arrhenius plots for both the samples and the activation energies E_a were calculated using the linear part. The introduction of Gd^{3+} slightly lowers the activation energy, but it appears that both the cathodes have a similar conduction mechanism as the difference in the E_a is slight.

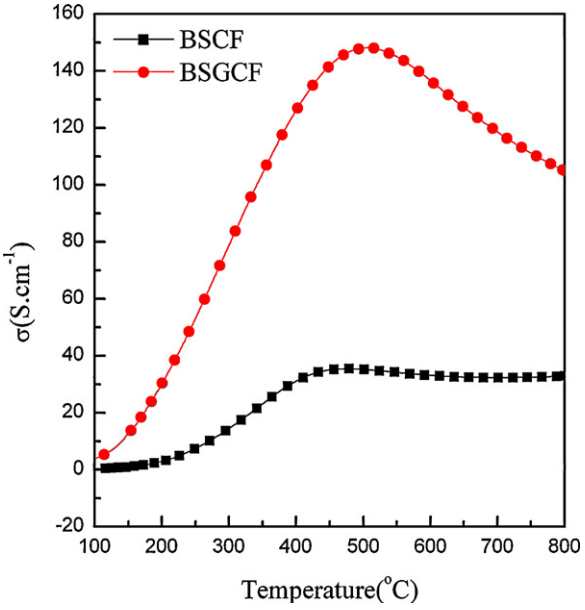

Fig. 4. Total electrical conductivities of BSCF and BSGCF as function of temperature in air.

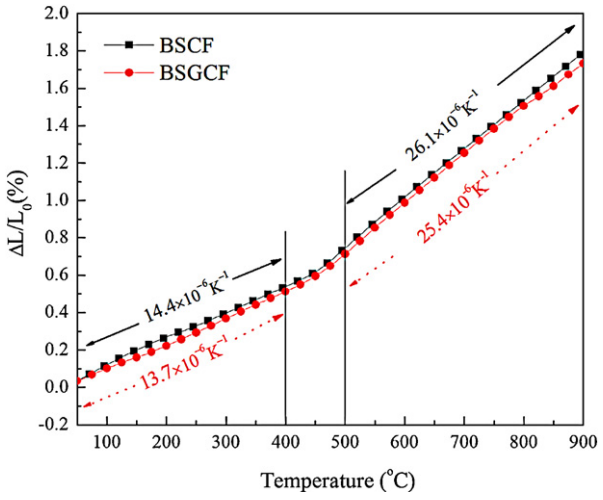

Fig. 3. Thermal expansion curves and specific TEC values for BSCF and BSGCF in air.

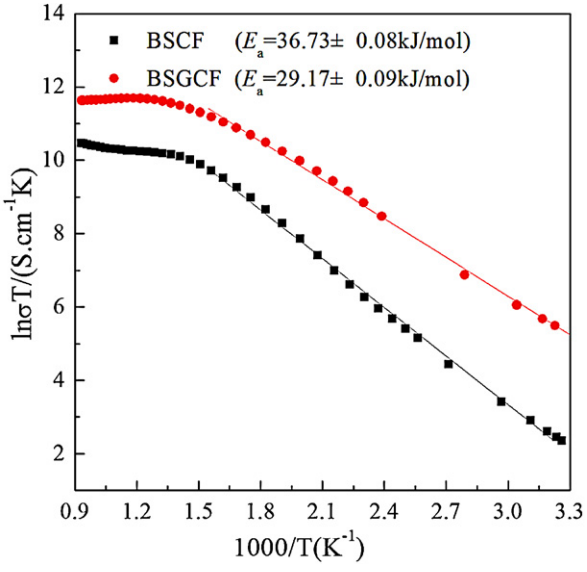

Fig. 5. Conductivities and calculated activation energies for BSCF and BSGCF samples in air.

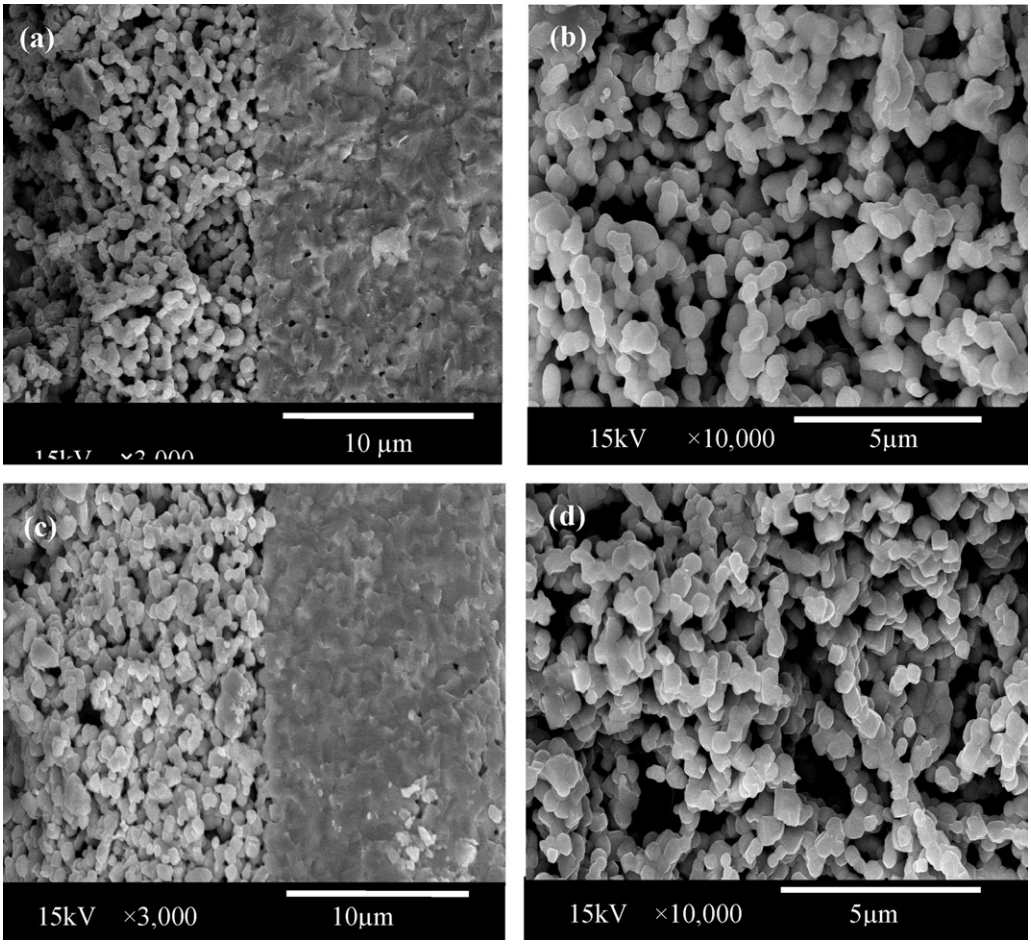

Fig. 6. SEM micrograph of the half-cells (SDC as electrolyte). Here (a) and (c) illustrate the cross-sections of BSCF and BSGCF as cathode, respectively; (b) and (d) illustrate the microstructures of the BSCF and BSGCF cathode, respectively.

3.5. Impedance spectra for symmetrical half cells

Fig. 6 shows the SEM morphologies of BSCF (a, b) and BSGCF (c, d) cathode calcined at 1000 °C for 4 h on a SDC electrolyte. Good adhesion can also be seen at the cathode|electrolyte interfaces. As shown in Fig. 6(b) and (d) of higher magnification image of the cathode, both the BSCF cathode (Fig. 6(b)) and BSGCF (Fig. 6(d)) are highly porous. The microscopic structure of BSGCF is similar to that of BSCF. Fig. 7 shows the AC impedance spectra at 500–650 °C in air for the BSCF and BSGCF. The impedance spectra of both cathodes can be separated into two arcs. This suggests that the oxygen reduction reaction on the electrodes contains at least two processes. The impedance spectra are fitted using the equivalent circuit in Fig. 7e. R_o represents the ohmic resistance, CPE is a constant phase element, R_1 corresponds to the high-frequency arc and R_2 is associated with a low-frequency arc. The high-frequency arc is associated with the charge-transfer process [33,34], while the low-frequency arc corresponds to the diffusion process, which includes adsorption–desorption of oxygen, oxygen diffusion at the gas-cathode surface interface and surface diffusion of intermediate oxygen species [35–38]. $R_{el} = R_1 + R_2$ is the overall polarization resistance of the electrodes. The effect of the A-site doping on the R_1 and R_2 at different temperatures is shown in Fig. 8. There is a significant decrease in the electrode polarization resistance by the Gd doping and the decrease is especially pronounced in the low-frequency arc. The R_2 of the diffusion process for BSGCF is 0.093 Ω cm^2 at 600 °C, 44.4% of that of BSCF. As mentioned above, the observed significant weight loss and the maximum electrical conductivity appear at 500–600 °C. For BSGCF oxides, the Gd doping induces the reduction of Fe^{4+} and Co^{4+} to Fe^{3+} and Co^{3+} to maintain the charge balance (Table 1). Thus the ability to the oxygen constraint is weakened, and this is beneficial to the oxygen diffusion. In addition to higher concentration of oxygen vacancies (V_o''), the higher electrical conductivity can also lead to the faster oxygen surface exchange [39]. Therefore, the decrease of R_2 with Gd doping can be expected.

3.6. Cell performance

Fig. 9 shows the performance of an anode-supported single cell with BSGCF cathode at 500–600 °C. Peak power densities as high as 236, 376, and 551 mW cm^{-2} are achieved at 500, 550, and 600 °C, respectively. The desirable

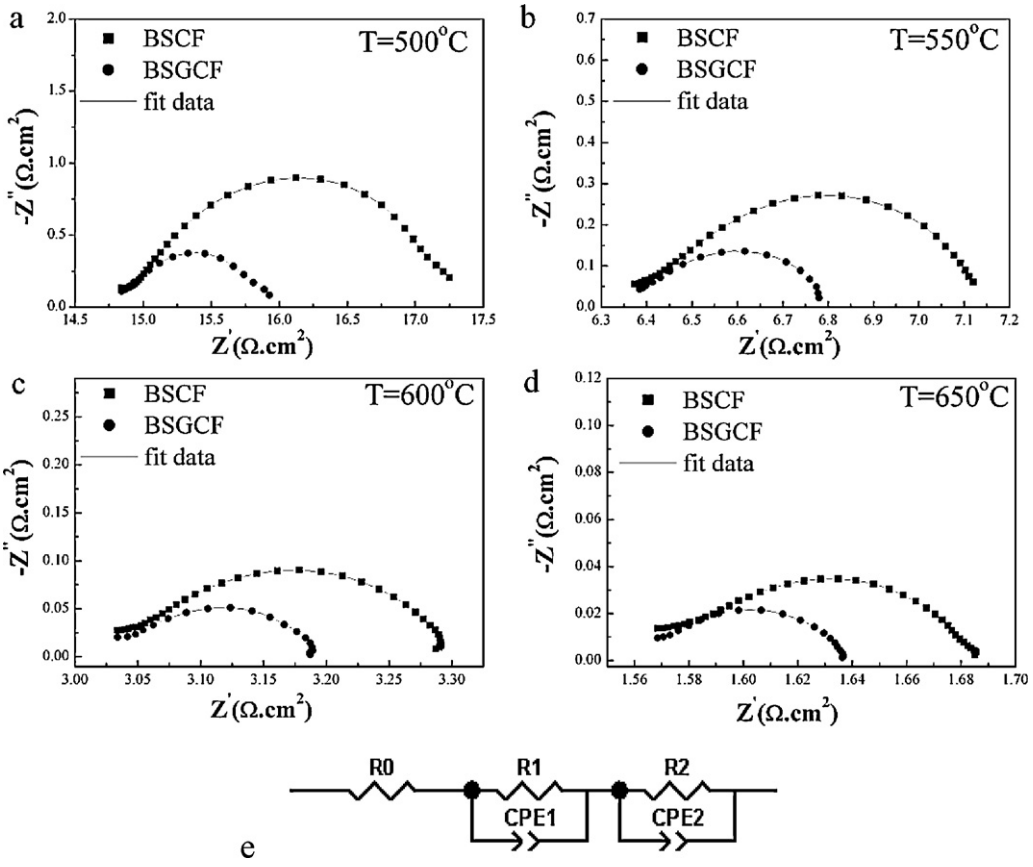

Fig. 7. The impedance spectra of symmetrical cells. The operating temperature was (a) 500 °C, (b) 550 °C, (c) 600 °C, (d) 650 °C, (e) equivalent circuit.

performance of the cell demonstrates that the BSGCF is a promising cathode for IT-SOFC. The AC-impedance of the cell was measured under the OCV conditions at temperatures ranging from 500 to 600 °C (Fig. 10). The ohmic resistance and the interfacial resistance of the cell are obtained from the impedance spectra (Fig. 11). The ohmic resistance decreases slowly but the interfacial resistance decreases dramatically with increasing temperature. The interfacial resistances of cell are 0.80, 0.33, and 0.16 Ω cm^2 at 500, 550, and 600 °C, respectively. Furthermore, other research results indicate that the interfacial polarization resistance for the oxidation reaction at the anode/electrolyte interface is relatively small [40,41]. This implies that oxygen reduction reaction at the cathode/electrolyte interface plays a major role in determining the cell performance. It is necessary to reduce the polarization resistance at cathode/electrolyte interface to improve the performance of the cell operating at intermediate temperatures [26].

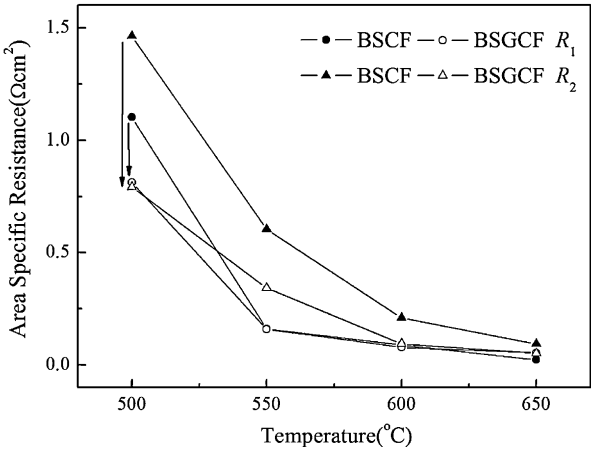

Fig. 8. Resistances of BSCF and BSGCF at 500, 550, 600 and 650 °C.

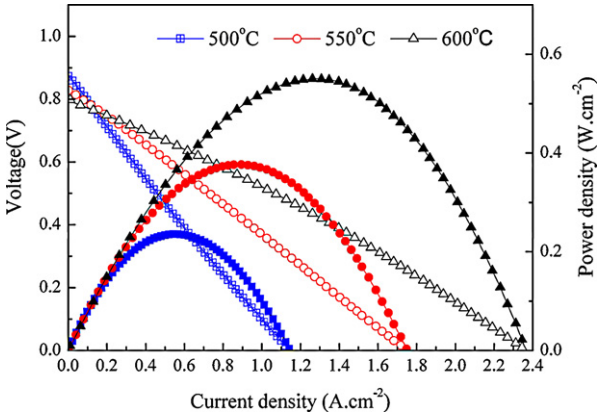

Fig. 9. The *I–V* and *I–P* curves of BSGCF/SDC/Ni-SDC single cell from 500 to 600 °C.

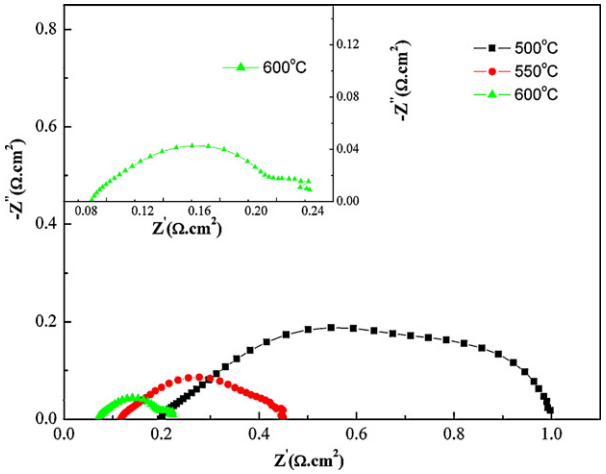

Fig. 10. Impedance spectra of the BSGCF/SDC/Ni-SDC single cell under open-circuit condition.

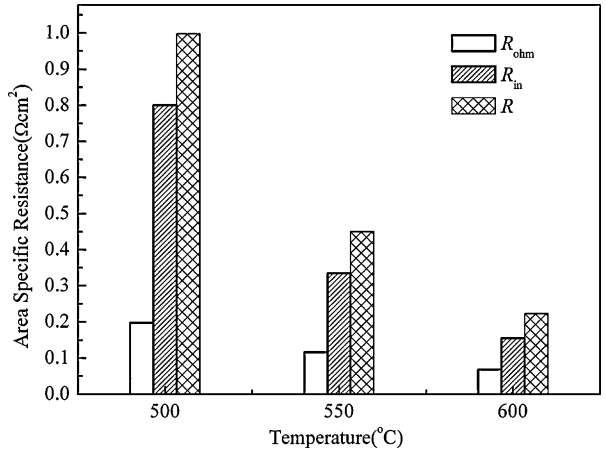

Fig. 11. Fitted data of impedance spectra for BSGCF/SDC/Ni-SDC single cell.

4. Conclusions

In this paper, a comparative study between the BSGCF and BSCF was carried out, including the phase structure, oxygen content ($3-\delta$), thermal expansion, electrical conductivity and electrochemical performance behaviors. The Gd doping in A-site of BSCF improve the electrical conductivity, oxygen nonstoichiometry δ and electrochemical properties, and decrease the TEC. The resistance associated with the diffusion processes for BSGCF is 0.093 Ω cm^2 at 600 °C, only 44.4% that of BSCF. The peak power density of ∼551 mW cm^{-2} is obtained for a thin-film electrolyte cell with BSGCF cathode at 600 °C. BSGCF is expected as a promising candidate cathode material for IT-SOFCs.

Acknowledgements

This research was supported by the National Natural Science Foundation of China (50902032 and 20901020) and Project (HIT.NSRIF.2009057) supported by Natural Scientific Research Innovation Foundation in Harbin Institute of Technology.

References

[1] K.C. Wincewicz, J.S. Cooper, Taxonomies of SOFC material and manufacturing alternatives, J. Power Sources 140 (2005) 280–296.
[2] N. Brandon, B. Skinner, B. Steele, Recent advances in materials for fuel cells, Ann. Rev. Mater. Res. 33 (2003) 183–213.
[3] Y. Leng, S.H. Chan, Q. Liu, Development of LSCF-GDC composite cathodes for low-temperature solid oxide fuel cells with thin film GDC electrolyte, Int. J. Hydrogen Energy 33 (2008) 3808–3817.
[4] H. Moon, S. Kim, S.Hyun, H. Kim, Development of IT-SOFC unit cells with anode-supported thin electrolytes via tape casting and co-firing, Int. J. Hydrogen Energy 33 (2008) 1758–1768.
[5] J. Mizusaki, J. Tabuchi, T. Matsuura, S. Yamauchi, K. Fueki, Electrical conductivity and seebeck coefficient of nonstoichiometric $La_{1-x}Sr_xCoO_{3-\delta}$, J. Electrochem. Soc. 136 (1989) 2082–2088.
[6] Y. Teraoka, H. Zhang, K. Okamoto, N. Yamazoe, Mixed ionic-electronic conductivity of $La_{1-x}Sr_xCo_{1-y}FeyO_{3-\delta}$ perovskite-type oxides, Mater. Res. Bull. 23 (1988) 51–58.
[7] S. Sekido, H. Tachibana, Y. Yamamura, T. Kambara, Electric–ionic conductivity in perovskite-type oxides, $Sr_xLa_{1-x}Co_{1-y}Fe_yO_{3-\delta}$, Solid State Ionics 37 (1990) 253–259.
[8] O. Yamamoto, Y. Takeda, R. Kanno, M. Noda, Perovskite-type oxides as oxygen electrodes for high temperature oxide fuel cells, Solid State Ionics 22 (1987) 241–246.
[9] H. Tu, Y. Takeda, N. Imanishi, O. Yamamoto, $Ln_{0.4}Sr_{0.6}Co_{0.8}Fe_{0.2}O_{3-\delta}$ (Ln = La, Pr, Nd, Sm, Gd) for the electrode in solid oxide fuel cells, Solid State Ionics 117 (1999) 277–281.
[10] Z. Shao, W. Yang, Y. Cong, H. Dong, G. Xiong, Investigation of the permeation behavior and stability of a $Ba_{0.5}Sr_{0.5}Co_{0.8}Fe_{0.2}O_{3-\delta}$ oxygen membrane, J. Membr. Sci 172 (2000) 177–188.
[11] Z. Shao, S. Haile, A high-performance cathode for the next generation of solid-oxide fuel cells, Nature 431 (2004) 170–173.
[12] W. Zhou, R. Ran, Z. Shao, Progress in understanding and development of $Ba_{0.5}Sr_{0.5}Co_{0.8}Fe_{0.2}O_{3-\delta}$-based cathodes for intermediate-temperature solid-oxide fuel cells: a review, J. Power Sources 192 (2009) 231–246.
[13] E. Magnone, A systematic literature review on BSCF-based cathodes for solid oxide fuel cell applications, J. Fuel Cell Sci. Technol. 7 (2010) 1–11.
[14] B. Wei, Z. Lü, S. Li, Y. Liu, K. Liu, W.##W. Su, Thermal and electrical properties of new cathode material $Ba_{0.5}Sr_{0.5}Co_{0.8}Fe_{0.2}O_{3-\delta}$ for solid oxide fuel cells, Electrochem. Solid State Lett. 8 (2005) A428–A431.
[15] Z. Talaei, H. Salamati, A. Pakzad, Fabrication and investigation of electrochemical characterization of Ba based cathodes, Int. J. Hydrogen Energy 35 (2010) 9401–9404.
[16] L. Tai, M. Nasrallah, H. Anderson, D. Sparlin, S.R. Sehlin, Structure and electrical properties of $La_{1-x}Sr_xCo_{1-y}Fe_yO_3$. Part 2. The system $La_{1-x}Sr_{x}$-$Co_{0.2}Fe_{0.8}O_3$, Solid State Ionics 76 (1995) 273–283.
[17] R. Su, Z. Lü, K. Chen, N. Ai, S. Li, B. Wei, W. Su, Novel in situ method (vacuum assisted electroless plating) modified porous cathode for solid oxide fuel cells, Electrochem. Commun. 10 (2008) 844–847.
[18] W. Zhou, R. Ran, Z. Shao, R. Cai, W. Jin, N. Xu, J. Ahn, Electrochemical performance of silver-modified $Ba_{0.5}Sr_{0.5}Co_{0.8}Fe_{0.2}O_{3-\delta}$ cathodes prepared via electroless deposition, Electrochim. Acta 53 (2008) 4370–4380.
[19] W. Zhu, Z. Lü, S. Li, B. Wei, J. Miao, X. Huang, K. Chen, N. Ai, W. Su, Study on $Ba_{0.5}Sr_{0.5}Co_{0.8}Fe_{0.2}O_{3-\delta}$-$Sm_{0.5}Sr_{0.5}CoO_{3-\delta}$ composite cathode materials for IT-SOFCs, J. Alloy Compd. 465 (2008) 274–279.
[20] N. Ai, S. Jiang, Z. Lü, K. Chen, W. Su, Nanostructured $(Ba,Sr)(Co,Fe)O_{3-\delta}$ impregnated $(La,Sr)MnO_3$ cathode for intermediate-temperature solid oxide fuel cells, J. Electrochem. Soc. 157 (2010) B1033–B1039.
[21] S. Li, Z. Lü, X. Huang, B. Wei, W. Su, Thermal, electrical, and electrochemical properties of lanthanum-doped $Ba_{0.5}Sr_{0.5}Co_{0.8}Fe_{0.2}O_{3-\delta}$, J. Phys. Chem. Solid 68 (2007) 1707–1712.
[22] S. Li, Z. Lü, X. Huang, W. Su, Thermal electrical, and electrochemical properties of Nd-doped $Ba_{0.5}Sr_{0.5}Co_{0.8}Fe_{0.2}O_{3-\delta}$ as a cathode material for SOFC, Solid State Ionics 178 (2008) 1853–1858.

[23] S. Li, Z. Lü, B. Wei, X. Huang, J. Miao, G. Cao, R. Zhu, W. Su, A study of $(Ba_{0.5}Sr_{0.5})_{1-x}Sm_xCo_{0.8}Fe_{0.2}O_{3-\delta}$ as a cathode material for IT-SOFCs, J. Alloy Compd. 426 (2006) 408–414.

[24] S. Li, Z. Lü, B. Wei, X. Huang, J. Miao, Z. Liu, W. Su, Performances of $Ba_{0.5}Sr_{0.5}Co_{0.6}Fe_{0.4}O_{3-\delta}$-$Ce_{0.8}Sm_{0.2}O_{1.9}$ composite cathode materials for IT-SOFC, J. Alloy Compd. 448 (2008) 116–121.

[25] L. Rørmark, A. Mørch, K. Wiik, S. Stølen, T. Grande, Enthalpies of oxidation of $CaMnO_{3-\delta}$, $Ca_2MnO_{4-\delta}$ and $SrMnO_{3-\delta}$ deduced redox properties, Chem. Mater. 13 (2001) 4005–4013.

[26] N. Ai, Z. Lü, K. Chen, X. Huang, B. Wei, Y. Zhang, S. Li, X. Xin, X. Sha, W. Su, Low temperature solid oxide fuel cells based on $Sm_{0.2}Ce_{0.8}O_{1.9}$ films fabricated by slurry spin coating, J. Power Sources 159 (2006) 637–640.

[27] N. Ai, Z. Lü, K. Chen, X. Huang, X. Du, W. Su, Effects of anode surface modification on the performance of low temperature SOFCs, J. Power Sources 171 (2007) 489–494.

[28] J. Peña-Martínez, D. Marrero-López, J. Ruiz-Morales, P. Núñez, C. Sánchez-Bautista, A. Dos Santos-García, J. Canales-Vázquez, On $Ba_{0.5}Sr_{0.5}Co_{1-y}Fe_yO_{3-\delta}$ ($y = 0.1$–0.9) oxides as cathode materials for $La_{0.9}Sr_{0.1}Ga_{0.8}Mg_{0.2}O_{2.85}$ based IT-SOFCs, Int. J. Hydrogen Energy 34 (2009) 9486–9495.

[29] Z. Chen, R. Ran, W. Zhou, Z. Shao, S. Liu, Assessment of $Ba_{0.5}Sr_{0.5}Co_{1-y}Fe_yO_{3-\delta}$ ($y = 0.0$–1.0) for prospective application as cathode for IT-SOFCs or oxygen permeating membrane, Electrochim. Acta 52 (2007) 7343–7351.

[30] J. Jung, S. Misture, D. Edwards, Oxygen stoichiometry, electrical conductivity, and thermopower measurements of BSCF ($Ba_{0.5}Sr_{0.5}Co_xFe_{1-x}O_{3-\delta}$ $0 \leq x \leq 0.8$) in air, Solid State Ionics 181 (2010) 1287–1293.

[31] S. Adler, Chemical expansivity of electrochemical ceramics, J. Am. Ceram. Soc. 84 (2001) 2117–2119.

[32] J. Jung, S. Misture, D. Edwards, Seebeck coefficient and electrical conductivity of BSCF ($Ba_{0.5}Sr_{0.5}Co_xFe_{1-x}O_{3-\delta}$ $0 \leq x \leq 0.8$) as a function of temperature and partial oxygen pressure, Solid State Ionics, doi:10.1016/j.ssi.2011.09.023, in press.

[33] F. Heuveln, H. Bouwmeester, Electrode properties of Sr-doped $LaMnO_3$ on yttria-stabilized zirconia, J. Electrochem. Soc. 144 (1997) 134–140.

[34] Y. Leng, S. Chan, K. Khor, S. Jiang, Performance evaluation of anode-supported solid oxide fuel cells with thin film YSZ electrolyte, Int. J. Hydrogen Energy 29 (2004) 1025–1033.

[35] M. Jørgensen, M. Mogensen, Impedance of solid oxide fuel cell LSM/YSZ composite cathodes, J. Electrochem. Soc. 148 (2001) A433–A442.

[36] S. Adler, Mechanism and kinetics of oxygen reduction on porous $La_{1-x}Sr_xCoO_{3-\delta}$ electrodes, Solid State Ionics 111 (1998) 125–134.

[37] S. Adler, J. Lane, B. Steele, Electrode kinetics of porous mixed-conducting oxygen electrodes, J. Electrochem. Soc. 143 (1996) 3554–3564.

[38] X. Chen, S. Chan, K. Khor, Simulation of a composite cathode in solid oxide fuel cells, Electrochim. Acta 49 (2004) 1851–1861.

[39] S. Adler, Factors governing oxygen reduction in solid oxide fuel cell cathodes, Chem. Rev. 104 (2004) 4791–4843.

[40] S. Souza, S. Visco, L. De Jonghe, Reduced-temperature solid oxide fuel cell based on YSZ thin-film electrolyte, J. Electrochem. Soc. 144 (1997) L35–L37.

[41] C. Xia, M. Liu, Microstructures, conductivities, and electrochemical properties of $Ce_{0.9}Gd_{0.1}O_2$ and GDC-Ni anodes for low-temperature SOFCs, Solid State Ionics 152 (2002) 423–430.